Editors' Suggestion

# Spin orbit torque driven magnetization reversal in CoFeTaB/Pt probed by resonant x-ray reflectivity

D. M. Burn,[1] R. Fan,[1] O. Inyang,[2] M. Tokaç,[2,3] L. Bouchenoire,[4,5] A. T. Hindmarch,[2] and P. Steadman[6]

[1]*Diamond Light Source, Harwell Science and Innovation Campus, Didcot OX11 0DE, United Kingdom*
[2]*Department of Physics, Durham University, South Road, Durham DH1 3LE, United Kingdom*
[3]*Department of Fundamental Sciences, Alanya Alaaddin Keykubat University, 07450 Antalya, Turkey*
[4]*XMaS, The UK-CRG Beamline, ESRF, 71 Avenue des Martyrs, CS 40220, F-38043 Grenoble, France*
[5]*Department of Physics, University of Liverpool, Liverpool L69 7ZE, United Kingdom*
[6]*Diamond Light Source, Didcot OX11 0DE, United Kingdom*

(Received 17 June 2022; accepted 22 August 2022; published 23 September 2022)

Resonant soft-x-ray reflectivity and vibrating sample magnetometry have been used to characterize field driven and spin orbit torque driven magnetization reversal in a CoFeTaB/Pt bilayer. Reversal of the magnetization occurs either along the applied field direction or perpendicular to the current flow direction. Magnetometry results show that field driven (current driven) coercivities are reduced by application of a current (field) highlighting the roles played by the two external parameters. In the current switching case, it is demonstrated with soft-x-ray hysteresis loops that only the layers near the interface with Pt switch, possibly highlighting the role of proximity effects of the magnetized Pt. We show how magnetization reversal perpendicular to the beam results in hysteresis behavior in the reflected intensity that is dependent on the magnetization but independent of the helicity of the circular polarization of the incident beam.

DOI: 10.1103/PhysRevB.106.094429

## I. INTRODUCTION

The interactions between the magnetization in a magnetic material and an electrical current are governed by the spin orbit interaction. As well as being a popular area for scientific study, the potential for the development of novel technological devices is significant. The spin orbit torque driven magnetization reversal shows promise for the development of future technological devices such as magnetic random access memory and magnetic logic devices [1–3]. The ability to manipulate magnetization through the application of electrical current or voltage is a developing field [4]. Systems with a magnetic layer and a layer with high spin orbit coupling give rise to interesting interfacial effects. An electrical charge current in the high spin orbit layer generates a transverse spin current. This spin current exerts a "spin orbit torque" (SOT) on magnetic moments in an adjacent magnetic layer and can manipulate the magnetization in the ferromagnetic layer [5–9].

A proximity-induced magnetism (PIM) frequently arises in nominally nonmagnetic layers interfaced with a magnet [10,11], determined by the interfacial magnetism in the magnetic layer [12]. In the high spin orbit material systems used for SOT, this PIM has an asymmetric influence on "interfacial spin-mixing conductance," which parametrizes spin-current transport across such interfaces [13]: When spin current is directed from the high spin orbit layer into the magnetic layer, as in SOT, the PIM makes no difference to the spin current transmission [14], whereas when it is directed from the magnetic layer into the high spin orbit layer, as in "spin-pumping," the PIM does have an impact [15,16]. The PIM also potentially has a further impact on electrical current flowing in the high spin orbit layer, generating a transverse conductivity via the anomalous Hall effect (AHE) in the proximity magnetized region.

Recently, Ding *et al.* found two competing contributions to the transverse conductivity in a Pt film on ferrimagnetic insulator TmIG [17]. These were explained as one term arising from the spin-Hall magnetoresistance, deriving from the interfacial spin-mixing conductance and representative of the "bulk" magnetic behavior of TmIG, and another due to the AHE in proximity magnetized Pt, representative of the interfacial magnetic behavior of TmIG. Interestingly, the two contributions are found to have different behavior during field driven reversal of the TmIG magnetization.

The nature of soft ferromagnetic/high spin-orbit coupled heterostructures lends itself to the study by soft-x-ray reflectivity. This technique has the ability to probe the element-specific magnetization as a function of depth through a multilayered structure resolving the magnetization orientation in both the layers and at the interfaces. Reflectivity measurements are strongly sensitive to structural changes from the electron density as a function of depth through the sample. However, additional modification to the scattering parameters originates due to magnetic scattering effects where magnetic contrast arises due to differences in the absorption of polarized x-rays [18]. Magnetic scattering ef-

*Published by the American Physical Society under the terms of the Creative Commons Attribution 4.0 International license. Further distribution of this work must maintain attribution to the author(s) and the published article's title, journal citation, and DOI.*

fects have been used to determine the magnetic structure from crystals [19–21] and also from magnetic heterostructures [10,22,23].

In this work, we use resonant soft-x-ray reflectivity to compare both the field driven and spin orbit torque driven magnetization reversal behavior in a CoFeTaB/Pt bilayer structure.

## II. EXPERIMENT

The $Co_{32}Fe_{32}Ta_{20}B_{16}$(6 nm)/Pt(3 nm) thin-film bilayer sample was prepared by dc magnetron sputtering under Ar working gas in an ultrahigh-vacuum deposition system. The $Co_{32}Fe_{32}Ta_{20}B_{16}$ (CoFeTaB) layer was deposited from an alloy sputtering target of the stated nominal composition (at. %), and the substrate was a Si(001) wafer with 100 nm thermally grown insulating $SiO_2$ coating. The CoFeTaB layer was deposited directly onto the wafer and then immediately capped with Pt. Deposition rates of around 0.02 nm/s were determined using a quartz crystal microbalance, and layer thicknesses were confirmed by postdeposition x-ray reflectivity measurements. The initial sample was then diced into individual pieces used for the various measurements presented here; confocal deposition geometry with sample rotation provides thickness uniformity over the initial sample area.

CoFeTaB is an amorphous ferromagnetic alloy where the saturation magnetization and Curie temperature can be tuned with the abundance of Ta [12]; 20 at. % Ta leads to a Curie temperature in excess of 100°C. The amorphous structure of CoFeTaB leads to a high electrical resistivity (200 $\mu$-Ohm cm), meaning that to a good approximation it can be assumed that electrical current in the bilayer structure flows only through the Pt layer (15–20 $\mu$-Ohm cm) [24]. In combination with the relatively low saturation magnetization of CoFeTaB, it is anticipated that this should result in efficient SOT driven magnetization reversal with a low critical current density.

Resonant soft-x-ray reflectivity measurements were performed in the RASOR diffractometer on the I10 beamline at Diamond Light Source [25]. The sample size was $1 \times 10$ mm and mounted on the cryostat arm of the diffractometer with its long axis aligned along the beam direction. The x-ray beam with a size of $100 \times 100$ $\mu$m was incident upon the sample at grazing angles and had an elongated footprint at the sample position. The beam was reflected from the sample, and the intensity of the specular reflectivity was measured with a photodiode orientated in a coupled $\theta$-$2\theta$ geometry. Slits on the $2\theta$ arm before the photodiode define the angular resolution of the measurements to 0.2°. In addition to the reflectivity, the incident x-rays excite electrons within the sample, which relax through fluorescent emission. This fluorescence was recorded simultaneously with a second photodiode positioned away from the reflected beam at a distance of 208 mm at an angle of 30° from the surface normal.

The reflectivity measurements were performed with polarized soft x-rays tuned to the Co $L_3$ absorption edge at 777 eV. The incident polarization was controlled using a six-axis insertion device [26], and measurements were performed with left- and right-circular polarization (LCP and RCP) along with both linear vertical ($\sigma$) and linear horizontal ($\pi$) polarizations. These combinations allow the probing of the various scattering matrix components which determine the reflected intensity. In this experiment, the polarization of the outgoing beam was not measured, and the reflectivity measurements therefore show a sum over all outgoing polarizations.

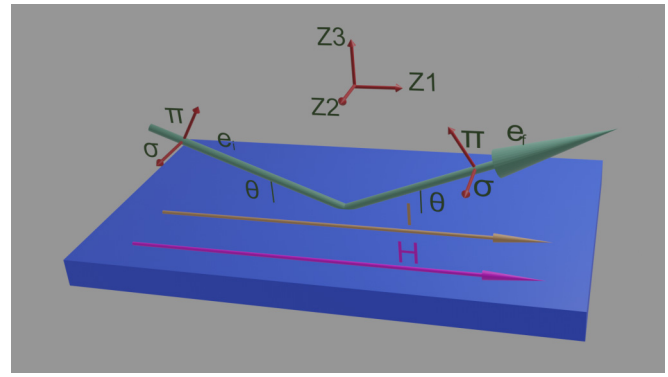


FIG. 1. Reflectivity measurements geometry, where $\mathbf{e_i}$ and $\mathbf{e_f}$ are the incoming and outgoing polarizations, and $\theta$ is the grazing angle of incidence and exit angle ($2\theta$ is the scattering angle). The arrows $I(H)$ show the direction of the applied current (magnetic field). $\pi$ and $\sigma$ represent polarization components parallel and perpendicular to the scattering plane, respectively.

A pair of electromagnet coils were used to supply an external magnetic field to the sample. This field was orientated within the plane of the sample and in the scattering plane. Electrical currents were also applied to the sample through contacts on either end of the sample such that the current flow was along the long axis of the sample, in the sample plane, and also in the scattering plane. The geometry of the experimental setup is illustrated in Fig. 1. Both the field and the current were applied to the sample individually with a sinusoidal waveform with a frequency of 1 Hz, and the quasistatic magnetization state was measured by averaging over multiple hysteresis loop cycles. This approach allowed measurements to be performed faster, and mitigated against any intensity drift in the incident beam intensity. Furthermore, this approach allowed the measurements to be performed with an effectively constant power load on the sample during the current driven measurements, and also on the electromagnet coils. Additional measurements as a function of current, with a constant field, and measurements as a function of field in a constant current were also performed for comparison. Throughout all the measurements, the temperature of the sample was maintained at 300 K to compensate for any Ohmic heating from the sample.

Resonant x-ray magnetic reflectivity measurements to probe proximity-induced magnetism in the Pt layer were also performed using the BM28 XMaS beamline at ESRF. Due to the element specificity of resonant scattering, these measurements are sensitive only to magnetism in Pt, which is induced due to proximity to an adjacent ferromagnet [12], and which we expect to be located close to the CoFeTaB/Pt interface only. The monochromatic, linearly polarized, incident x-ray beam had energy tuned close to the Pt $L_3$ absorption edge (11.569 keV), and a diamond phase plate was used to induce circular polarization (~90%) [27]. The sample magne-

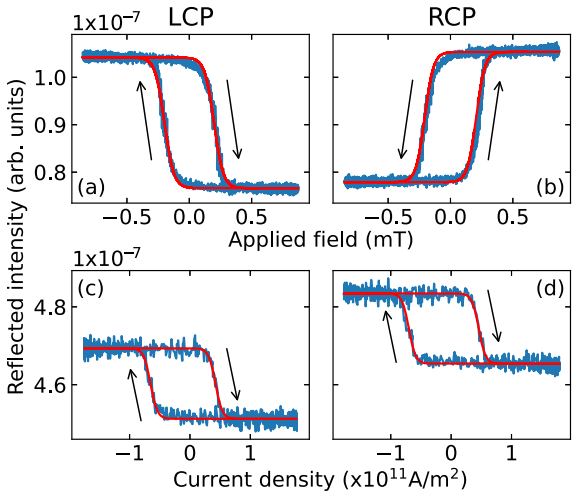


FIG. 2. Specular reflectivity from a CoFeTaB-Pt bilayer as a function of (a), (b) applied field and (c),(d) applied current. Measurements are at the Co $L_3$ absorption edge with both left- and right-circularly polarized x-rays (left and right columns, respectively). Measurements are performed at an angle of $\theta = 10^\circ$ ($Q_z = 0.13$ Å$^{-1}$) and the red lines show tanh fits to the transitions in intensity. The arrows indicate the direction of the ramps in reflected intensity.

tization was reversed between positive (+) and negative (−) applied magnetic field giving polarized reflectivities $R^+$ and $R^-$. The x-ray magnetic reflectivity (XRMR) is $(R^+ + R^-)/2$, which only contains structural contributions, and the XRMR asymmetry is $(R^+ - R^-)/(R^+ + R^-)$, which contains the contribution from magnetic scattering. Asymmetry measurements are made with both left- and right-hand incident circular polarization; the magnetic asymmetry signal reverses with the helicity. The data were analyzed using GenX software [28].

In addition to the x-ray study, the samples were also characterized using a superconducting quantum interference device vibrating sample magnetometer (SQUID-VSM) using smaller $1 \times 2$ mm sections of the sample. Complementary to the soft-x-ray study, measurements of the magnetization as a function of field were performed with an additional dc current applied parallel to the magnetic field axis. The magnetization was also probed along the same axis.

## III. RESULTS

Soft-x-ray reflectivity measurements were performed at the Co $L_3$ edge. This was found from the energy that gave the biggest difference in fluorescence intensity between measurements with opposite circular polarization. At this energy, the reflected intensity provides an element-specific probe of the magnetization within the ferromagnetic layer in the CoFeTaB/Pt bilayers. We initially measure this reflected intensity as a function of the magnetic field with no applied current. These measurements reveal the hysteresis loops shown by the examples in Figs. 2(a) and 2(b) at an incidence angle of $\theta = 10^\circ$.

The field driven hysteresis loop shape is relatively sharp, with a small coercivity. This shape is typical for a soft ferromagnetic material and indicates magnetization reversal between two distinct saturated states. Measurements with left- and right-circularly polarized x-rays provide inverted contrast to the magnetization. This results in the inversion of the hysteresis loop shape between panels (a) and (b) in Fig. 2.

Figures 2(c) and 2(d) show the reflected intensity where the magnetization state is manipulated by an applied current through the sample in zero external magnetic field. A similar hysteresis loop behavior is observed in the reflected intensity where switching between two clear states occurs when the current exceeds a critical current density.

In contrast to the field driven loops, we find that the sign of the current driven loops is not inverted when comparing the intensity measured with the opposite circular polarization. Furthermore, we note that the reflected intensity in the two saturated states is different for the two polarizations. We will discuss these features in more detail later.

The hysteresis loops have been further analyzed by fitting the data with tanh functions to represent the transition between the two saturated states. These are indicated by the red lines overlaid on the data in Fig. 2. The reflected intensity at the two saturated states, $s1$ and $s2$, as well as the coercivity $H_c$ or the critical current for reversal and a parameter representing the shape of the transition were all extracted from the fit parameters. These parameters provide the data shown in the rest of the analysis in this manuscript.

The x-ray reflectivity measured during both field and current driven hysteresis loops was measured for a range of reflectivity angles. This is shown in Fig. 3(a) for both of the saturated states, $s1$ and $s2$, as a function of the momentum transfer, $Q_z$. Again, the measurements were performed at the Co $L_3$ edge and repeated with both left- and right-circularly polarized light.

All the lines show a typical reflectivity curve shape with a $Q^4$ decrease in intensity coupled with Kiessig fringes resulting from interference effects between the layers. In addition to the strong structural contributions to the reflectivity signal, magnetic scattering effects lead to an additional modulation of the signal, as also seen in Fig. 2. The difference in intensity between the two saturated states is shown more clearly as the asymmetry in Fig. 3(b). This asymmetry is defined as the difference divided by the sum of the two intensities, and it allows for a comparison over a large dynamic range in the reflected intensity. The asymmetry between the different pairs of reflectivity measurements for both field and current driven loops measured with both left- and right-circularly polarized light is compared.

The asymmetry between the reflected intensities from the two saturated states obtained from field driven loops is shown by the dashed lines in Fig. 3(b). This signal contains large variations as a function of $Q_z$ with a periodicity linked to that of the Kiessig fringes. When measurements are compared with opposite circular polarization, the asymmetry shows the same behavior with an inverted sign.

In comparison, the reflectivity curves from the two current driven states share many similarities. Again there is a decrease in reflected intensity as a function of $Q_z$, with Kiessig fringes at a periodicity matching that of the field driven reflectivity measurements. This similarity is expected as the structure of the film dominates the reflectivity signal and remains the same

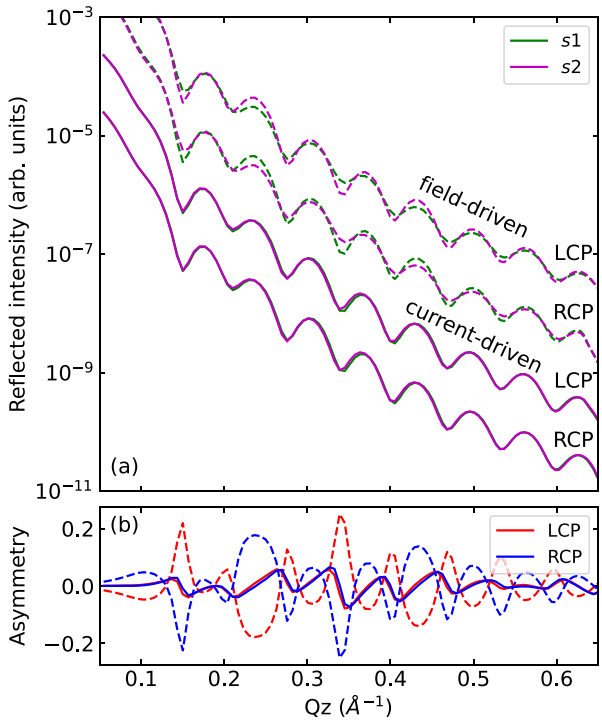


FIG. 3. (a) Specular reflectivity intensity from a CoFeTaB-Pt bilayer as a function of the momentum transfer $Q_z$ measured at the Co $L_3$ edge. The intensities from the two saturated magnetization states, $s1$ and $s2$, were obtained from fits to hysteresis loops driven by either applied magnetic field (dashed lines) or electrical current (solid lines). The measurements are shown with both left and right circular polarization (LCP and RCP, respectively), and pairs of curves ($s1$ and $s2$) are shifted by $\times 10$ for clarity. (b) The asymmetry, $[(s1 - s2)/(s1 + s2)]$, between the reflected intensities from the different states as a function of $Q_z$ shown for both field and current driven states and measured with both polarizations.

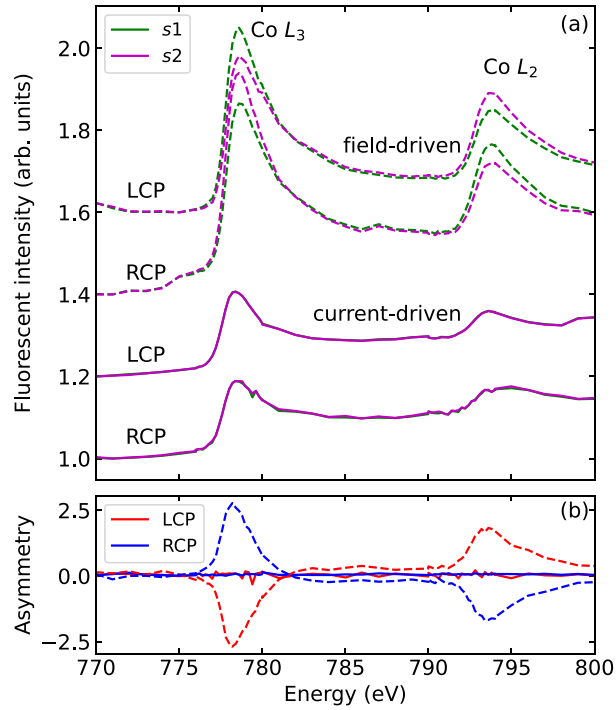


FIG. 4. (a) Fluorescent intensity from a CoFeTaB-Pt bilayer as a function of incident x-ray energy at a fixed x-ray incidence angle of $\theta = 10^\circ$ ($Q_z = 0.13$ Å$^{-1}$). Intensities are shown for the two saturated magnetic states, $s1$ and $s2$, obtained from fits to field driven (dashed) and current driven (solid) hysteresis loops. Measurements with both left and right circular polarization (LCP and RCP, respectively) are compared, and pairs of curves ($s1$ and $s2$) are shifted by $\times 10$ for clarity. (b) The asymmetry, $[(s1 - s2)/(s1 + s2)]$, between the fluorescent intensities, also as a function of energy.

when the magnetism is manipulated by either the applied field or the current. However, the asymmetry between the curves in Fig. 3(b) reveals details resulting from the differences in magnetic structure between the two states. Again, the asymmetry varies as a function of $Q_z$ with the same periodicity of the Kiessig fringes, however there is no change in the asymmetry when inverting the polarization of the incident x-rays. This occurs over the entire measured $Q_z$ range. The absence of the inversion in the asymmetry is representative of the consistency of the hysteresis loop shape when varying the incident polarization, as seen in Figs. 2(c) and 2(d).

The reflectivity measurements provide insight into the detailed depth dependence of both the structure and the magnetization through the sample. At the Co edge, this probe is expected to extend up to 100 nm into the sample, probing the entire sample stack [29], and the contrast arises due to a combination of factors including x-ray absorption and polarization-dependent scattering effects. In addition to the reflectivity, the x-ray induced fluorescence from the sample was also measured. This provides a measure of the x-ray absorption, revealing the projection of the magnetization onto the incident beam direction, which is independent of any scattering phenomenon.

The fluorescence intensity variations between the current and field driven states are best illustrated in Fig. 4 as a function of incident beam energy. Following a similar process, we measure the intensity as a function of either field or current and fit the hysteresis loops to extract parameters $s1$ and $s2$ representing the intensity in the two saturated states. These measurements are repeated at each energy with both left- and right-circularly polarized x-rays.

In all cases, we observe a peak in the x-ray fluorescence at both the $L_3$ and $L_2$ absorption edges in Co at 777 and 794 eV, respectively. In the field driven case, there is a clear difference in the fluorescence and the related asymmetry from the two oppositely magnetized states. Furthermore, we observe an inversion of the asymmetry when changing the circular polarization, and we also observe an inversion of the sign of the asymmetry when comparing the $L_3$ and $L_2$ edges.

In contrast to the field driven switching, the x-ray fluorescence spectra appear quite different when driving the system using the applied current. First, the x-ray fluorescence spectra appear distorted, with lower intensity at each absorption edge. This modification may suggest a change in the $L_{3,2}$ transition when a spin-polarized current is flowing in the Pt layer. Furthermore, there is no measurable difference in fluorescence between the two saturated states at either the $L_3$ or $L_2$ edge.

The strong dichroism in the fluorescence signal at the $L_{2,3}$ absorption edges, the inversion of the sign of the dichroism

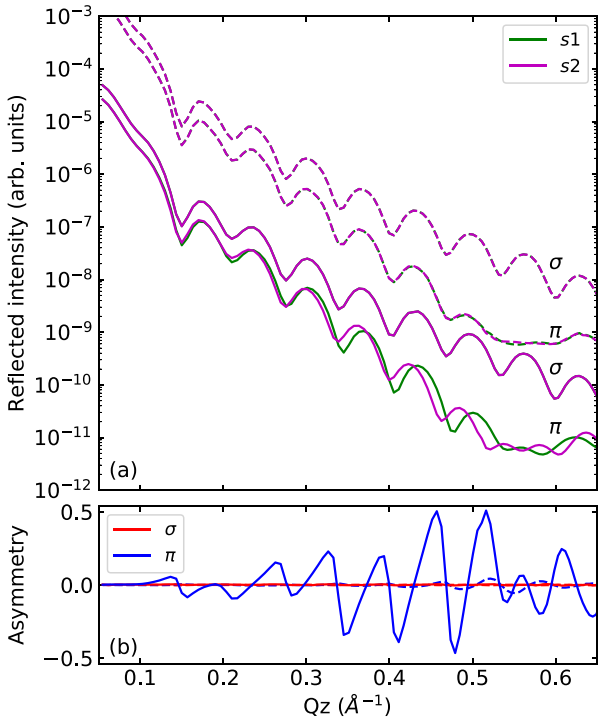


FIG. 5. (a) Specular reflectivity intensity from a CoFeTaB-Pt bilayer as a function of the momentum transfer $Q_z$ measured at the Co $L_3$ edge. The intensities, $s1$ and $s2$, from the saturated states were extracted from fits to field driven (dashed lines) and current driven (solid lines) hysteresis loops. Measurements are repeated with $\sigma$ and $\pi$ linearly polarized light, and pairs of curves are shifted by $\times 10$ for clarity. (b) The asymmetry, $[(s1 - s2)/(s1 + s2)]$, between the reflected intensities also shown as a function of $Q_z$.

between $L_3$ and $L_2$, and also that between measurements with left- and right-circularly polarized light are all consistent with field driven magnetization reversal with a dominating component along the incident beam direction [30]. This supports the reflectivity measurements. However, the contrast from the reflectivity measurements, accompanied by the lack of any asymmetry in the fluorescence between the current driven states, indicates that magnetization reversal is taking place in this system along an axis with no projection onto the incident beam direction. This suggests a current driven reorientation of the magnetization perpendicular to the incident beam direction that is expected to be in-plane in the sample due to the strong anisotropy associated with the thin film.

In addition to the reflectivity measurements with circularly polarized light, measurements were also performed with both vertical, $\pi$, and horizontal, $\sigma$, linear polarized light. Here the contributions to the scattering are more complex, with components of the magnetic scattering matrix revealing greater sensitivity towards magnetization components that lie on axes perpendicular to the beam propagation direction [19].

Figure 5 shows the specular reflectivity from the saturated states extracted from both field and current driven hysteresis loops measured with both $\sigma$- and $\pi$-polarized x-rays. As in Fig. 3, the reflectivity is sensitive to the layered structure of the films giving rise to the characteristic x-ray reflectivity pattern with Kiessig fringes. When probed with $\pi$-polarized light, the intensity becomes extinct at $Q_z = 0.55$ Å$^{-1}$. Here the charge scattering is zero at the Brewster angle, but magnetic scattering still remains [19].

With field driven magnetization reversal, only a small asymmetry is observed with $\pi$-polarized light towards higher $Q_z$ values, and no asymmetry is observed with $\sigma$-polarized light. This is consistent with the circular polarized x-ray reflectivity in Fig. 3, suggesting a strong magnetization alignment along the applied field direction which lies in the scattering plane.

The current driven magnetization reversal shows a significant asymmetry when probed with $\pi$-polarized light. These measurements indicate the presence of a magnetization that is aligned perpendicular to the beam propagation direction.

The reflectivity and fluorescence results indicate that the magnetization in the CoFeTaB/Pt bilayer can be manipulated by both an external magnetic field and also using the electrical current. With the field, the magnetization reversal is along the field direction. The projection of this magnetization onto the beam direction gives rise to the signal in the reflectivity with circular polarized light and also a difference in the fluorescence resulting from dichroic absorption. The current acts to align the magnetization perpendicular to the current flow direction, with no change in net magnetization projection along the beam direction resulting in no difference in the fluorescence. Furthermore, magnetization in this geometry results in a strong asymmetry in the reflectivity with linearly polarized light.

The behavior of the reflectivity with circular polarized light with the current driven magnetization is interesting as an asymmetry between the two magnetized states is still observed without any change in projection of the magnetization along the beam direction. This difference in intensity is also unusual as it is not symmetric and the contrast is not inverted when changing the polarization. This can be further understood by considering the change in the resonant magnetic scattering form factor [19],

$$f = (\varepsilon' \cdot \varepsilon)F^{(0)} - i(\varepsilon' \times \varepsilon) \cdot MF^{(1)}. \quad (1)$$

Here $\varepsilon'$ and $\varepsilon$ are the incoming and outgoing polarization, respectively, $M$ is the magnetic moment, and the $F^{(0)}$ and $F^{(1)}$ are dependent on the transitions and atomic properties. Circular polarization can be represented in terms of light parallel to the scattering plane, $\pi$, and perpendicular, $\sigma$. Here one handedness is represented by $\sigma + i\pi$ and the opposite by $\sigma - i\pi$. By inserting these into the above equation, it can be seen that $f$ has a linear dependence on the magnetization. The scattering should therefore show a clear hysteresis loop as a function of applied field (or current). It can also be shown that if the magnetization is in the scattering plane, the loops can be inverted when the helicity is inverted. It is interesting to note that if the magnetization vector is perpendicular to the scattering plane, while the measured hysteresis loops do not invert with helicity, they remain sensitive to the sample magnetization.

To understand the data shown in Fig. 2, we have simulated the expected reflectivity at the Co $L_3$ edge at $\theta = 10^\circ$ from the bilayer using the magneto-optics model developed by Zak [31–33] and the scattering form factor from the x-ray

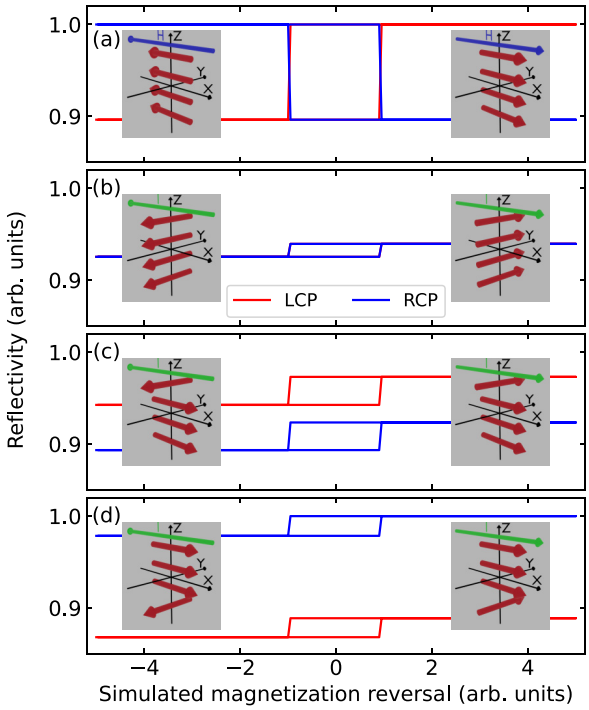


FIG. 6. Models showing the reflected intensity from a CoFeTaB/Pt bilayer as a function of an effective field or current for left- and right-circularly polarized x-rays (LCP and RCP), at the Co $L_3$ edge and at an incidence angle of $\theta = 10^\circ$. The entire magnetization in the 6 nm magnetic layer is switched (a) parallel and (b) perpendicular to the beam. Partial magnetization reversal in the (c) top and (d) bottom 1.5 nm of a 6.0-nm-thick magnetic layer where the remaining magnetization remains pinned along the beam axis. The insets illustrate the orientation of the magnetic moment direction with respect to the incident x-ray beam.

interaction database [29]. The results of our simulations show that for the field driven loop in Fig. 6(a), where the magnetic moments follow the applied magnetic field and rotate along the x-ray propagation direction, we observe a hysteresis loop shape with inverted contrast when changing between left- and right-circularly polarized light. In the case of current driven loops, where the magnetic moments switch within the sample plane and perpendicular to the current and x-ray probe direction, Fig. 6(b) shows the hysteresis loop shape with no dependence on the helicity of the circular polarization.

Furthermore, Figs. 6(c) and 6(d) show the simulated intensity for a sample in which only a fraction of the magnetic layer experiences the magnetization reversal while the rest remains pinned along the beam direction. In Fig. 6(c) only the top 2 nm, and in Fig. 6(d) only the bottom 2 nm of the 12 nm ferromagnetic layer is reversed. The shift in intensity between the loops is reminiscent of the shift observed in the experimental current driven loops in Figs. 2(c) and 2(d) and suggests that the spin orbit torque driven reversal acts with local proximity to the upper interface with the Pt layer where the torque is applied to the ferromagnetic layer.

The importance of the role of the CoFeTaB-Pt interface is also highlighted through reflectivity measurements at the Pt $L_3$ edge, which are shown in Fig. 7. Similarly to the soft-x-ray reflectivity, Fig. 7(a) shows the reflected intensity as a function of angle, while Fig. 7(b) shows the asymmetry in the magnetic reflectivity, measured with opposite circularly polarized light.

The reflectivity data have been fitted to a layered model for the $SiO_2$/CoFeTaB/Pt structure. The structural scattering length density profile for this model is shown in Fig. 7(c) as a function of depth through the film. In addition to the structural scattering length density, the modeling reveals the magnetic scattering length density profile associated with the element-specific magnetic depth profile within the Pt layer, which is illustrated by the red line in Fig. 7(c). Here, a peak at the CoFeTaB/Pt interface is consistent with the proximity-induced magnetism (PIM) in heavy metal layers [10,12,34]. The PIM in Pt has been shown not to have any influence on SOT driven magnetization reversal [14], but the PIM provides an important proxy measurement for the interfacial magnetic behavior in CoFeTaB. The presence of a PIM in the Pt layer indicates that there is no magnetic "dead-layer" at the CoFeTaB/Pt interface, and the interface magnetization lies predominantly in the sample plane and along the beam direction—the direction to which XRMR is sensitive. The interfacial region in the CoFeTaB layer is ferromagnetic and magnetized in the sample plane along the direction of the "bulk" layer magnetization. The reversal of the spin-asymmetry, Fig. 7(b), on switching incident helicity

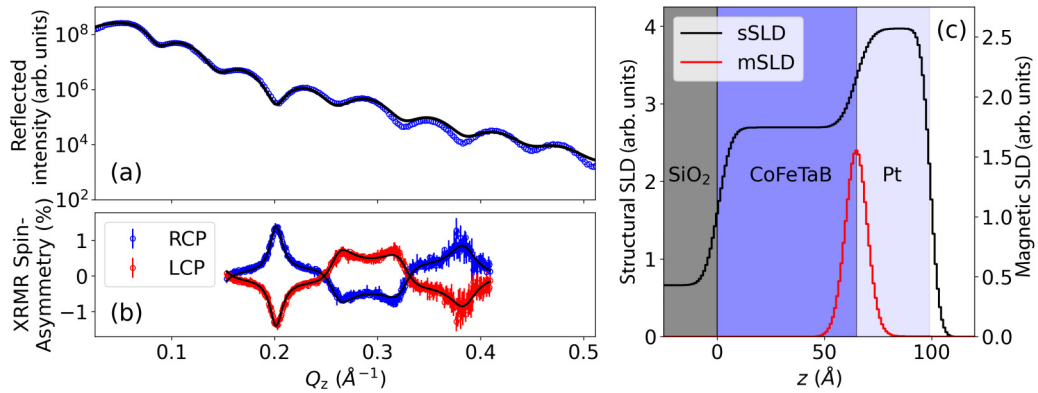


FIG. 7. X-ray reflectivity (a) and spin asymmetry (b) for the CoFeTaB/Pt sample measured at the Pt $L_3$ absorption edge at 11.569 keV. The solid lines represent the best fit to the data from a layered model illustrated by the structural (black) and magnetic (red) scattering length density profile (c).

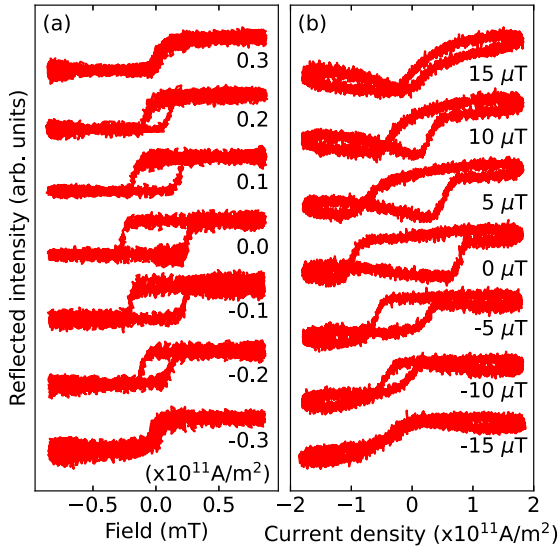


FIG. 8. Reflected intensity from a CoFeTaB/Pt bilayer measured with right-circularly polarized light at the Co $L_3$ edge at an incidence angle of $\theta = 10^\circ$. (a) Loops measured as a function of magnetic field at a range of fixed current densities. (b) Loops measured as a function of current density with fixed magnetic field.

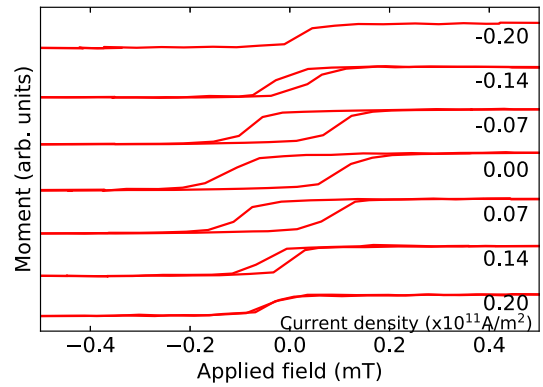


FIG. 9. Field driven hysteresis loops measured by VSM-SQUID magnetometry with a dc current applied parallel to the measurement and applied field direction. Loops are offset for clarity.

from LCP to RCP suggests that in the field driven case the PIM, and hence also interfacial CoFeTaB magnetization, follows the bulk layer magnetization of CoFeTaB—as depicted in Fig. 6(a).

With the knowledge of the magnetic moments direction, we can also understand the observations in Fig. 5, i.e., the observed change in scattering intensity is dominated by the interference between the charge and $\pi$-$\pi$ magnetic scattering. Even though the $\sigma$-polarized light has a magnetic contribution from $\sigma$-$\pi$ scattering, the amplitude is small and it is below the detection level of our experiment, therefore the $\sigma$ reflectivity is insensitive to the magnetic moments direction. When the system is driven by a magnetic field, the magnetic moments following the magnetic field result in no changes in the overall scattering form factor, hence there is no change in the observed reflectivity. In the current driven scenario, the magnetic moments rotate perpendicular to the x-ray propagation direction. This changes the sign of the magnetic form factor, causing a notable change in the magnetic scattering. Furthermore, the largest changes of the asymmetry are observed around the Brewster angle. This is due to the nonmagnetic form factor being close to zero near the Brewster angle, and therefore the intensity is dominated by the magnetic scattering resulting in maximum asymmetry. Finally, the lack of asymmetry in current driven fluorescence in Fig. 4 is to be expected as the absorption cross section for circular light is identical for magnetic moments perpendicular to the x-ray propagation direction.

In addition to the purely field or current driven loops, the effect of a dc offset on the loop behavior has also been considered. Figure 8(a) shows field driven hysteresis loops measured with a dc applied current, while Fig. 8(b) shows current driven hysteresis loops measured with a dc applied field.

With a dc current, Fig. 8(a) shows field driven hysteresis loops that experience a reduction in the coercivity as a function of the applied current. This is symmetrical for both current directions and is dependent only on the magnitude of the current. The temperature of the sample is maintained at 300 K during all measurements, and therefore any thermal effects assisting in the field driven reversal can be neglected. With the dc current, an additional torque is applied to the moments due to the spin orbit torque. This additional torque reduces the external field required for field driven magnetization reversal, and it results in a reduction in the coercivity. Since the spin orbit torque acts perpendicular to the field direction, a current in either direction results in a reduction in the coercivity for both increasing and decreasing field sweep directions.

The current driven loops in Fig. 8(b) show a reduction in the critical current needed for current driven switching when assisted by the dc magnetic field. This can be explained through a similar approach in which the torque required for magnetization is effectively reduced by the application of the dc field. In addition to the reduction of the critical field, Fig. 8 shows that the transitions between states are broadened.

These loops also show an asymmetry where for the right circular polarized x-rays shown in Fig. 8(b) the positive fields shift the transitions in the loops towards higher currents, and the negative fields shift the transitions towards lower currents. When left circular polarized x-rays are used, this shift is reversed. While there is no circular dichroism measured in the current driven hysteresis loops in zero field, the combination of both current and field reveals coupling between the current and the magnetization of the sample when both are applied simultaneously.

Complementary measurements of the magnetization as a function of field were performed on the CoFeTaB-Pt sample using a VSM-SQUID magnetometer. Figure 9 shows hysteresis loops of the magnetization as a function of field where a current is applied to the sample parallel to the field direction, in the same geometry as for the x-ray reflectivity measurements. Again, the current modifies the hysteresis loop shape, leading to a reduction in the coercivity and a closing of the hysteresis loop shape.

The results from the VSM-SQUID are important as not only do they support the x-ray measurements, but they also

rule out any potential effects that could be attributed to heating from the x-ray beam.

## IV. CONCLUSIONS

In conclusion, the field driven magnetization reversal in a CoFeTaB/Pt bi-layer has been measured with x-ray reflectivity, x-ray fluorescence, and VSM-SQUID magnetometry. These measurements show a typical ferromagnetic hysteresis loop with two magnetized states orientated along the field direction. A current applied through the CoFeTaB/Pt bilayer also results in magnetization reversal within the ferromagnetic layer through spin orbit torque effects. This effect is consistent with modeling indicating the reversal of the near-interface region of the ferromagnetic layer in close proximity to the interface with the Pt layer. The lack of asymmetry in fluorescence absorption measurements, and a strong reflectivity asymmetry with linear polarized light, indicate magnetization reversal perpendicular to the current flow direction. We observe hysteresis loops in the reflectivity measured with circular polarized light which do not invert in contrast when changing between left and right circular polarization, which is also attributed to perpendicular magnetization reversal.

In combination, the applied field and spin orbit torques act to reduce either the coercivity or critical current density required for switching. These measurements are also supported by corresponding VSM-SQUID magnetometry and demonstrate the potential for x-ray reflectivity techniques to provide an important layer- and interface-resolved probe of spin orbit torque effects.

## ACKNOWLEDGMENTS

We acknowledge support from Nigerian government TET-Fund scheme (OI), Republic of Turkey Ministry of National Education (MT), EPSRC Grant Ref. No. EP/L000121/1, HEFCE ODA, and the Royal Society (ATH). XMaS is a UK national research facility supported by EPSRC. We thank Diamond Light Source for the provision of I10 beamtime and SQUID-VSM access.

[1] P. Gambardella and I. M. Miron, Current-induced spin-orbit torques, Philos. Trans. R. Soc. A **369**, 3175 (2011).

[2] K. Jabeur, G. Di Pendina, F. Bernard-Granger, and G. Prenat, Spin orbit torque non-volatile flip-flop for high speed and low energy applications, IEEE Electron Device Lett. **35**, 408 (2014).

[3] R. L. Stamps, S. Breitkreutz, J. Åkerman, A. V. Chumak, Y. Otani, G. E. Bauer, J. U. Thiele, M. Bowen, S. A. Majetich, M. Kläui, I. L. Prejbeanu, B. Dieny, N. M. Dempsey, and B. Hillebrands, The 2014 magnetism roadmap, J. Phys. D **47**, 333001 (2014).

[4] J. C. Slonczewski, Current-driven excitation of magnetic multilayers, J. Magn. Magn. Mater. **159**, L1 (1996).

[5] I. M. Miron, G. Gaudin, S. Auffret, B. Rodmacq, A. Schuhl, S. Pizzini, J. Vogel, and P. Gambardella, Current-driven spin torque induced by the Rashba effect in a ferromagnetic metal layer, Nat. Mater. **9**, 230 (2010).

[6] K. Garello, I. M. Miron, C. O. Avci, F. Freimuth, Y. Mokrousov, S. Blügel, S. Auffret, O. Boulle, G. Gaudin, and P. Gambardella, Symmetry and magnitude of spin-orbit torques in ferromagnetic heterostructures, Nat. Nano. **8**, 587 (2013).

[7] T. D. Skinner, M. Wang, A. T. Hindmarch, A. W. Rushforth, A. C. Irvine, D. Heiss, H. Kurebayashi, and A. J. Ferguson, Spin-orbit torque opposing the Oersted torque in ultrathin Co/Pt bilayers, Appl. Phys. Lett. **104**, 062401 (2014).

[8] T. Nan, S. Emori, C. T. Boone, X. Wang, T. M. Oxholm, J. G. Jones, B. M. Howe, G. J. Brown, and N. X. Sun, Comparison of spin-orbit torques and spin pumping across NiFe/Pt and NiFe/Cu/Pt interfaces, Phys. Rev. B **91**, 214416 (2015).

[9] C. Kim, B. S. Chun, J. Yoon, D. Kim, Y. J. Kim, I. H. Cha, G. W. Kim, D. H. Kim, K. W. Moon, Y. K. Kim, and C. Hwang, Spin-orbit torque driven magnetization switching and precession by manipulating thickness of CoFeB/W heterostructures, Adv. Electron. Mater. **6**, 1901004 (2020).

[10] J. Geissler, E. Goering, M. Justen, F. Weigand, G. Schütz, J. Langer, D. Schmitz, H. Maletta, and R. Mattheis, Pt magnetization profile in a pt/co bilayer studied by resonant magnetic x-ray reflectometry, Phys. Rev. B **65**, 020405(R) (2001).

[11] F. Wilhelm, P. Poulopoulos, G. Ceballos, H. Wende, K. Baberschke, P. Srivastava, D. Benea, H. Ebert, M. Angelakeris, N. K. Flevaris, D. Niarchos, A. Rogalev, and N. B. Brookes, Layer-resolved Magnetic Moments in Ni/Pt Multilayers, Phys. Rev. Lett. **85**, 413 (2000).

[12] O. Inyang, L. Bouchenoire, B. Nicholson, M. Tokaç, R. M. Rowan-Robinson, C. J. Kinane, and A. T. Hindmarch, Threshold interface magnetization required to induce magnetic proximity effect, Phys. Rev. B **100**, 174418 (2019).

[13] Y. Tserkovnyak, A. Brataas, G. E. W. Bauer, and B. I. Halperin, Nonlocal magnetization dynamics in ferromagnetic heterostructures, Rev. Mod. Phys. **77**, 1375 (2005).

[14] L. J. Zhu, D. C. Ralph, and R. A. Buhrman, Irrelevance of magnetic proximity effect to spin-orbit torques in heavy-metal/ferromagnet bilayers, Phys. Rev. B **98**, 134406 (2018).

[15] M. Caminale, A. Ghosh, S. Auffret, U. Ebels, K. Ollefs, F. Wilhelm, A. Rogalev, and W. E. Bailey, Spin pumping damping and magnetic proximity effect in pd and pt spin-sink layers, Phys. Rev. B **94**, 014414 (2016).

[16] C. Swindells, H. Głowiński, Y. Choi, D. Haskel, P. P. Michałowski, T. Hase, P. Kuświk, and D. Atkinson, Proximity-induced magnetism and the enhancement of damping in ferromagnetic/heavy metal systems, Appl. Phys. Lett. **119**, 152401 (2021).

[17] S. Ding, Z. Liang, C. Yun, R. Wu, M. Xue, Z. Lin, A. Ross, S. Becker, W. Yang, X. Ma, D. Chen, K. Sun, G. Jakob, M. Kläui, and J. Yang, Anomalous hall effect in magnetic insulator heterostructures: Contributions from spin-hall and magnetic-proximity effects, Phys. Rev. B **104**, 224410 (2021).

[18] B. T. Thole, P. Carra, F. Sette, and G. van der Laan, X-ray Circular Dichroism as a Probe of Orbital Magnetization, Phys. Rev. Lett. **68**, 1943 (1992).

[19] J. P. Hill and D. F. Mcmorrow, X-ray resonant exchange scattering: Polarization dependence and correlation functions, Acta Crystallogr. Sect. A Found. Crystallogr. **52**, 236 (1996).

[20] J. Fink, E. Schierle, E. Weschke, and J. Geck, Resonant elastic soft x-ray scattering, Rep. Prog. Phys. **76**, 056502 (2013).

[21] C. Detlefs, A. H. M. Z. Islam, A. I. Goldman, C. Stassis, P. C. Canfield, J. P. Hill, and D. Gibbs, Determination of magnetic-moment directions using x-ray resonant exchange scattering, Phys. Rev. B **55**, R680(R) (1997).

[22] S. Macke and E. Goering, Magnetic reflectometry of heterostructures, J. Phys.: Condens. Matter **26**, 363201 (2014).

[23] J. M. Tonnerre, L. Seve, D. Raoux, G. Soullie, B. Rodmacq, and P. Wolfers, Soft X-Ray Resonant Magnetic Scattering from a Magnetically Coupled Ag/Ni Multilayer, Phys. Rev. Lett. **75**, 740 (1995).

[24] O.-O. Inyang, Magnetic proximity effect and interfacial spin dependent transport in ferromagnet/heavy metal thin films, Ph.D. thesis, Durham University, 2018.

[25] T. A. Beale, T. P. Hase, T. Iida, K. Endo, P. Steadman, A. R. Marshall, S. S. Dhesi, G. Van Der Laan, and P. D. Hatton, RASOR: An advanced instrument for soft x-ray reflectivity and diffraction, Rev. Sci. Instrum. **81**, 073904 (2010).

[26] H. Wang, P. Bencok, P. Steadman, E. Longhi, J. Zhu, and Z. Wang, Complete polarization analysis of an APPLE II undulator using a soft x-ray polarimeter, J. Synch. Radiat. **19**, 944 (2012).

[27] L. Bouchenoire, S. Brown, P. Thompson, C. Detlefs, and M. Cooper, Polarisation optimisation for ferromagnetic diffraction: A case study of iron, Nucl. Instrum. Methods Phys. Res., Sect. A **566**, 733 (2006).

[28] M. Björck and G. Andersson, *GenX*: an extensible X-ray reflectivity refinement program utilizing differential evolution, J. Appl. Crystallogr. **40**, 1174 (2007).

[29] B. L. Henke, E. M. Gullikson, and J. C. Davis, X-ray interactions: Photoabsorption, scattering, transmission, and reflection at E = 50-30,000 eV, Z = 1-92, At. Data Nucl. Data Tables **54**, 181 (1993).

[30] G. van der Laan and A. I. Figueroa, X-ray magnetic circular dichroism: a versatile tool to study magnetism, Coord. Chem. Rev. **277-278**, 95 (2014).

[31] J. Zak, E. R. Moog, C. Liu, and S. D. Bader, Universal approach to magneto-optics, J. Magn. Magn. Mater. **89**, 107 (1990).

[32] J. Zak, E. R. Moog, C. Liu, and S. D. Bader, Magneto-optics of multilayers with arbitrary magnetization directions, Phys. Rev. B **43**, 6423 (1991).

[33] J. Zak, E. R. Moog, C. Liu, and S. D. Bader, Fundamental magneto-optics, J. Appl. Phys. **68**, 4203 (1990).

[34] R. M. Rowan-Robinson, A. A. Stashkevich, Y. Roussigné, M. Belmeguenai, S.-M. Chérif, A. Thiaville, T. P. A. Hase, A. T. Hindmarch, and D. Atkinson, The interfacial nature of proximity-induced magnetism and the dzyaloshinskii-moriya interaction at the pt/co interface, Sci. Rep. **7**, 16835 (2017).